frontiers in Earth Science

ORIGINAL RESEARCH
published: 15 April 2021
doi: 10.3389/feart.2021.652501

Neodymium Isotopes in Glauconite for Palaeoceanographic Reconstructions at Continental Margins: A Preliminary Investigation From Demerara Rise

Pierre Giresse[1], Germain Bayon[2]*, Cedric Tallobre[1] and Lies Loncke[1]*

[1] Centre de Formation et de Recherche sur les Environnements Méditerranéens (CEFREM), UMR 5110 CNRS, Université de Perpignan Via Domitia, Perpignan, France, [2] Centre de Bretagne, Institut Français de Recherche pour l'Exploitation de la Mer, Marine Geosciences Unit, Plouzané, France

OPEN ACCESS

Edited by:
Christian März,
University of Leeds, United Kingdom

Reviewed by:
Patrick Blaser,
University of Lausanne, Switzerland
Philipp Böning,
University of Oldenburg, Germany

****Correspondence:***
Pierre Giresse
giresse@univ-perp.fr
Germain Bayon
gbayon@ifremer.fr

Specialty section:
This article was submitted to Geochemistry, a section of the journal Frontiers in Earth Science

Received: *12 January 2021*
Accepted: *17 March 2021*
Published: *15 April 2021*

Citation:
Giresse P, Bayon G, Tallobre C and Loncke L (2021) Neodymium Isotopes in Glauconite for Palaeoceanographic Reconstructions at Continental Margins: A Preliminary Investigation From Demerara Rise. Front. Earth Sci. 9:652501. doi: 10.3389/feart.2021.652501

Contourite sediment accumulations at continental margins are related to strong bottom water circulation, where intense winnowing can result in neoformation of authigenic grains of glauconite at the seafloor. In this study, we investigated whether such glauconite grains could faithfully record ambient bottom-water neodymium (Nd) isotopic compositions, and hence be used as paleoceanographic archives. To this purpose, we measured Nd isotopic compositions (ε_{Nd}) in a series of glauconitic grains, foraminiferal assemblages, leached Fe-Mn oxyhydroxide phases, and detrital clays separated from a contourite sediment record at the Demerara slope off French Guiana (IG-KSF-11; 2370 m water depth), at a location where the present-day ε_{Nd} distribution along the water column is well characterised. We show that the ε_{Nd} composition of core-top glauconite grains (-12.0 ± 0.5) agrees with the expected NADW-like seawater signature at the same location and water depth (-11.6 ± 0.3), while departing from measured ε_{Nd} values for corresponding detrital clays (-11.3 ± 0.2), foraminiferal (-10.9 ± 0.2), and Fe-Mn oxyhydroxide fractions (-9.2 ± 0.2). This finding indicates that glauconitic grains at this particular location are probably best suited for paleoceanographic reconstructions than foraminifera and leached Fe-oxyhydroxide fractions, which appear to be influenced by sediment redistribution and the presence of terrestrial continental Fe-oxides, respectively. Using rare earth elements (REE), we tentatively propose that the acquisition of seawater Nd isotopic signatures by glauconite is controlled by the presence of authigenic REE-bearing phosphate-rich phases intertwined within clay mineral sheets, while confirming previous findings that the process of glauconitisation results in the progressive loss of REE within glauconitic grains. Preliminary paleoceanographic implications suggest strengthened bottom-water circulation of the glacial analogue of NADW at this particular location and water depth, with a ε_{Nd} signature (between -10.8 and -11.5) similar to that of modern NADW.

Keywords: rare earth elements, neodymium isotopes, glauconitisation, Demerara, contourite

INTRODUCTION

Since at least the beginning of the Neogene, the sedimentation at the Guianese margin of the Demerara Plateau has been controlled by large contour currents (Loncke et al., 2016; Tallobre et al., 2016; Fanget et al., 2020). At this location, slope bottom deposits are subject to recurrent winnowing that favours the appearance and mineralogical maturation of green glauconitic grains at the seawater–sediment interface (Tallobre et al., 2019). Each contourite sequence is characterised by high abundance of glauconitic grains (especially in the moat area), but also in a moderately to strongly discontinuous sediment accumulation associated with relatively low sedimentation rates. In contrast with nearby shallower settings along the French Guiana margin that have experienced continuous fine-grained hemipelagic sedimentation during the Late Quaternary (Häggi et al., 2017; Zhang et al., 2017; Crivellari et al., 2018), the Demerara contourite system, as other contourite deposits (e.g., Giresse and Wiewióra, 2001; Giresse, 2008), is characterised by deposition of discontinuous sediment records, which prevents their use for paleoceanographic reconstructions. Additionally, intense bottom current activity at Demerara and other contourite settings at continental margins can also result in substantial sediment redistribution, with potential effect on the reliability of commonly used paleoceanographic archives in marine sediment records.

The purpose of this study is to show the potential interest of using glauconitic grains in such discontinuous sedimentary records for paleoceanographic reconstructions based on radiogenic neodymium isotopes. Neodymium (Nd) isotopic ratios are commonly measured in biogenic material, such as fish teeth or foraminifer shells, or in the associated Fe-Mn oxyhydroxide fractions of the sediment, as tracers of bottom water circulation (e.g., Frank, 2002; Goldstein and Hemming, 2003). In the ocean, each water mass is tagged with a distinctive Nd isotopic composition (typically expressed using the epsilon notation $\varepsilon_{\mathrm{Nd}}$), which reflects, to a large extent, that of the continental masses surrounding their source region (e.g., Tachikawa et al., 2017; Robinson et al., 2021). While Nd isotopes have proven particularly helpful for reconstructing past ocean circulation patterns over various geological timescales, their application to contourite sediment accumulations at ocean margins, such as the Demerara Rise, can be skewed by sedimentary processes related to strong bottom current activity, such as winnowing and reworking.

In oceanic environments, glauconitic grains are the result of transformation and neoformation processes taking place at the water–sediment interface. Various granular supports (mudclasts, faecal pellets, and foraminifera infillings) include inherited 1:1 interstratified clays (or Te-Oc; i.e., clay minerals consisting of one tetrahedral sheet and one octahedral sheet, such as kaolinite) that become gradually replaced by 2:1 clays (Te-Oc-Te) dominated first by smectite, and then glauconite. These processes are accompanied by aluminium and silicium depletion in inherited minerals, together with significant enrichment of iron and potassium in neoformed minerals (e.g., Odin and Matter, 1981). While K in neoformed clays is supplied by ambient seawater, the source of Fe is most likely derived from reactive phases of the terrigenous sediment, such as Fe-oxide and oxyhydroxide phases (Odin and Matter, 1981; Odin and Fullagar, 1988; Giresse and Wiewióra, 2001; Wiewióra et al., 2001; Giresse, 2008; Banerjee et al., 2016). In all cases, these thermodynamic reactions operate at slow kinetic rates, especially regarding the acquisition of seawater-derived K, thereby requiring prolonged residence time at the water–sediment interface, presumably over thousands of years (e.g., Giresse, 1975), and thus reduced sedimentation rates. Earlier studies suggested that such conditions were mostly met at continental platforms, in particular at their outer edges, far from any continental source of terrigenous material. More recently, however, several investigations of contouritic deposits along continental margins revealed important glauconitic accumulations at water depths between ∼2000 and 3000 m (Giresse et al., 1998; Giresse and Wiewióra, 2001; Giresse, 2008; Stow and Faugères, 2008; Faugères and Mulder, 2011). Similar to continental shelf analogues, the occurrence of abundant glauconitic grains in contouritic systems indicates prolonged exposure at the water–sediment interface, reflecting here recurring sediment reworking related to the winnowing action of contouritic currents. Due to Fe incorporation, glauconite grains typically display higher specific gravity (between ∼2.4 and 2.9 g/cm^3; Yadav and Sharma, 1992) than the average surrounding sediment (∼1.7 g/cm^3; Tenzer and Gladkikh, 2014). As a consequence, authigenic grains of glauconite are less likely to be remobilised and dispersed by currents, compared to empty foraminiferal tests. Additionally, because glauconite formation occurs over relatively long timescales at the seawater–sediment interface, unlike other archives of bottom water chemistry (e.g., fish teeth and sedimentary Fe-Mn oxyhydroxide phases), glauconite grains could possibly integrate the signature of bottom water masses over prolonged periods of time (Giresse and Wiewióra, 2001; Giresse, 2008), which, while preventing their use in high-resolution studies, would provide an effective means for yielding reliable average estimates on past ε_{Nd} signatures of bottom water masses. To date, however, this hypothesis has never been tested.

To address this issue, we have investigated the Nd isotopic composition of glauconite grains recovered from contourite sediment deposits at Demerara Rise; at a location where ε_{Nd} signatures of modern water masses are already well characterised (Huang et al., 2014). This ε_{Nd} comparison extends to more conventional paleoceanographic archives (uncleaned foraminifers and leached sedimentary Fe-oxyhydroxide phases), being also complemented by the additional use of rare earth elements (REE) and major element ratios, such as K_2O/Al_2O_3 and Fe_2O/Al_2O_3. Since the different phases of glauconitisation include the transformation and neoformation of phyllosilicate minerals, a careful investigation is also required to assess the degree to which Nd isotopes in glauconite grains may reflect the detrital ε_{Nd} signature of inherited clay minerals within the sediment. Following proxy calibration using core-top sediments, preliminary interpretations will be made of a set of Nd isotopic data for buried glauconitic grains, in the light of the changing paleoceanographic context since the last glacial period.

MODERN AND PAST OCEANOGRAPHIC SETTING

This study focuses on an area of contourite accumulation located at Demerara Rise, along a regional slope failure headscarp, where the bottom current influence is the strongest, with flow velocity up to ∼30 cm/s (Tallobre et al., 2016; **Figure 1**). At this location (∼2400 m water depth), sedimentary dynamics is controlled by uneven accelerations of contour currents that define condensed intervals of deposits, or even lead to significant stratigraphic gaps in the sediment record (Loncke et al., 2016; Tallobre et al., 2016, 2019). Under such conditions, the application of both oxygen isotopes and radiocarbon chronostratigraphic methods has proven generally unreliable (Tallobre et al., 2019), yielding $\delta^{18}O$ depth profiles that cannot be directly tuned to nearby continuous records of hemipelagic sediments (Huang et al., 2014; Häggi et al., 2017).

The present-day distribution of radiogenic Nd isotopes along the water column at Demerara Rise identifies the presence of distinct water masses (**Figure 2**), including the West North Atlantic Central waters (WNACW; $\varepsilon_{Nd} \sim -13$), from surface to ∼500 m water depth, the Antarctic Intermediate Water (AAIW; $\varepsilon_{Nd} \sim -10.5$), between ∼ 500 and 1200 m depth, the North Atlantic Deep Water (NADW; ε_{Nd} from ∼ −12 to −11.5), from

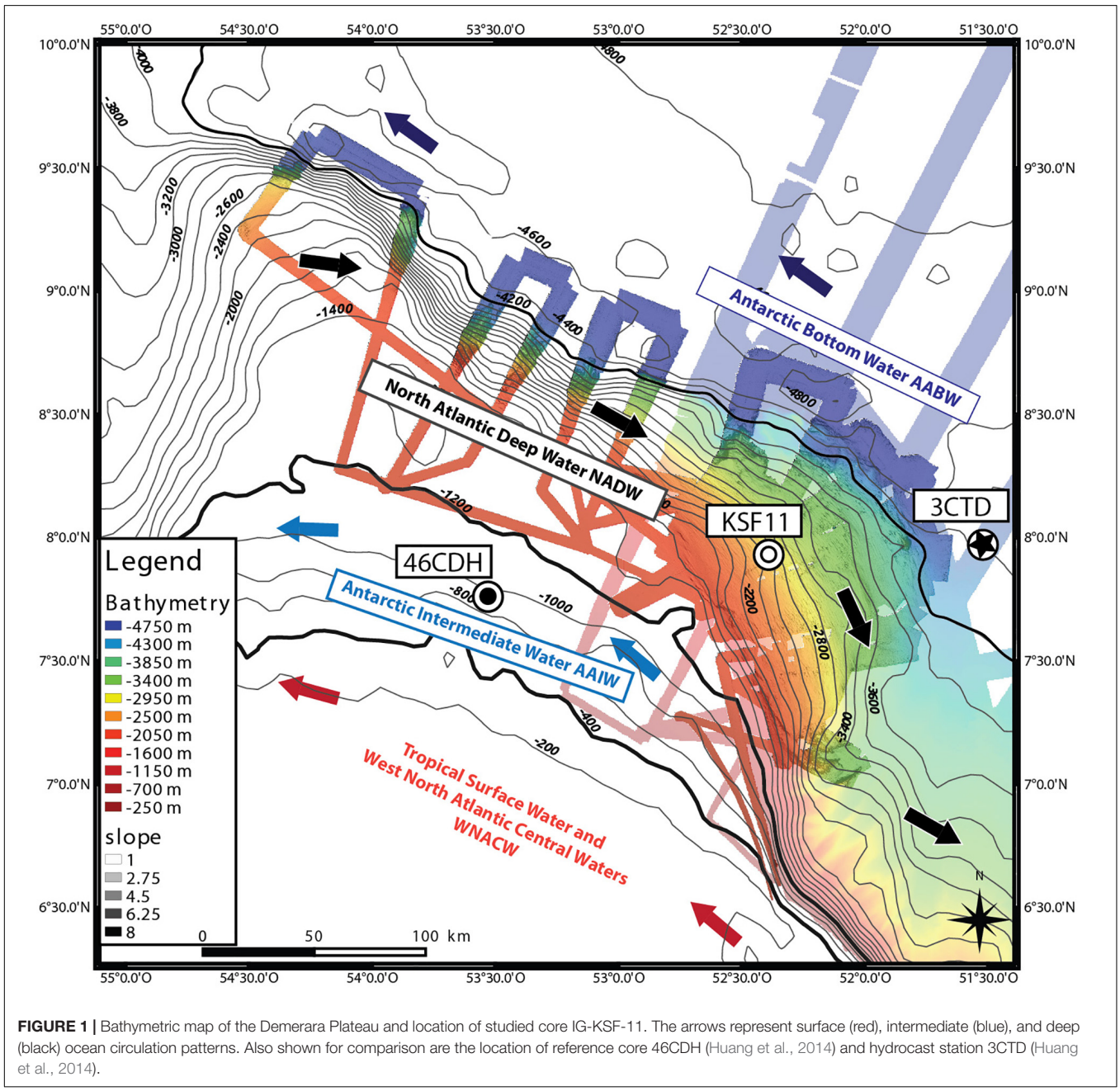

FIGURE 1 | Bathymetric map of the Demerara Plateau and location of studied core IG-KSF-11. The arrows represent surface (red), intermediate (blue), and deep (black) ocean circulation patterns. Also shown for comparison are the location of reference core 46CDH (Huang et al., 2014) and hydrocast station 3CTD (Huang et al., 2014).

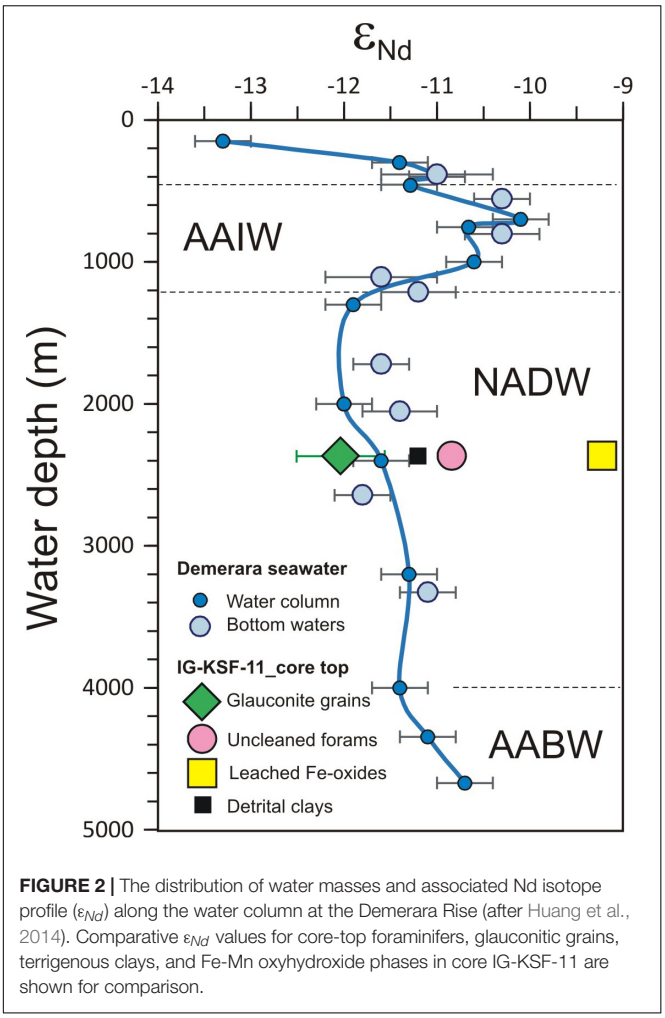

FIGURE 2 | The distribution of water masses and associated Nd isotope profile (ε_{Nd}) along the water column at the Demerara Rise (after Huang et al., 2014). Comparative ε_{Nd} values for core-top foraminifers, glauconitic grains, terrigenous clays, and Fe-Mn oxyhydroxide phases in core IG-KSF-11 are shown for comparison.

$\sim$ 1200 and 4000 m depth, and finally, the Antarctic Bottom Water (AABW; $\varepsilon_{Nd} \sim -10.5$) below 4000 m depth (Huang et al., 2014). In previous investigations, the application of Nd isotope measurements to various paleoceanographic archives retrieved from Demerara Rise (Huang et al., 2014) and other locations in the Atlantic have proven particularly useful to reconstruct past ocean circulation patterns, indicating prominent changes in the Atlantic Meridional Overturning Circulation (AMOC) over glacial–interglacial timescales, with impact on heat transport and carbon storage in the surface and deep ocean, respectively (e.g., Rutberg et al., 2000; Piotrowski et al., 2004, 2005; Pahnke et al., 2008; Böhm et al., 2015; Howe et al., 2016; Lippold et al., 2016; Pöppelmeier et al., 2020). A survey of the spatial distribution of Nd isotopes in the Atlantic during both the recent Holocene and the last glacial periods indicated relatively unradiogenic NADW-like ε_{Nd} values (~ -13) below 1500 m water depth at Demerara Rise (Howe et al., 2016). Further south in the Atlantic Ocean, the Nd isotopic composition of NADW becomes progressively more radiogenic, reflecting gradual dilution of northern-sourced waters with overlying and underlying Antarctic water masses (Howe et al., 2016). As a consequence, the unradiogenic "tongue" of NADW can be traced as the water mass flows southward in the South Atlantic at water depths between $\sim$2000 and 4000 m (e.g., von Blanckenburg, 1999; Howe et al., 2016). During the Last Glacial Maximum (LGM), the deep Atlantic water column displayed a greater influence of southern-sourced waters consistent with a reduced flux of NADW to the Southern Atlantic (Rutberg et al., 2000; Howe et al., 2016; Pöppelmeier et al., 2020). At the Demerara margin, Nd isotopic measurements were previously acquired on uncleaned foraminifera from a nearby sediment core collected at 947 m depth, bathed at present-day by AAIW (Huang et al., 2014; see core 46CDH on **Figure 1**). The obtained ε_{Nd} record for the past 25,000 years indicated similar Nd isotopic compositions during the Holocene and the LGM ($\varepsilon_{Nd} \sim -10$), while revealing pronounced ε_{Nd} excursions towards unradiogenic values (between -11 and -12) during the short-lived North Atlantic cold periods of the Heinrich Stadial 1 (HS1) and the Younger Dryas (YD), interpreted as reflecting strong reduction of the AMOC leading to reduced influence of northward flowing AAIW in the equatorial Atlantic (Huang et al., 2014).

MATERIALS AND METHODS

This study was conducted on sediment core IG-KSF-11 (07°51.85N, 052°29.25W; 2370 m water depth), recovered off French Guiana during the IGUANES cruise (R/V *L'Atalante;* Loncke L., 2013[1]). The sedimentary records retrieved from this dynamic sedimentary environment are characterised by the occurrence of abundant glauconite grains (Tallobre et al., 2019). The sediment is dominated by homogeneous grey-green silty mud with alternation of discrete sand layers (Tallobre et al., 2016, 2019). Core IG-KSF-11 was specifically chosen for this study because foraminifera $\delta^{18}O$ measurements suggest a continuous and coherent stratigraphy for the upper 0–80 cm sediment interval that is considered in this study (**Figure 3A**), which covers approximately the last 60,000 years BP (Tallobre et al., 2019). However, similar to the other sediment records retrieved from the Demerara contourite system, IG-KSF-11 suffers from inherent chronostratigraphic uncertainties due to the presence of recurrent winnowing and other erosional processes, resulting in hiatuses and frequent radiocarbon age inversions in the lower part of the core (from $\sim$2.5 to 6 m depth; Tallobre et al., 2019). As a consequence, in this study, the analysed sediment layers were only assigned a period of deposition (i.e., marine isotope stage 1, MIS 2. . .), rather than a precise stratigraphic age (**Tables 1**, **2**).

For this study, a series of glauconite grains and planktonic foraminifers were collected from six distinct sediment layers (0, 8, 20, 29, 40, and 70 cm) representative of specific time intervals (Holocene, MIS 2, MIS 3) in core IG-KSF-11. Evidence for continuous stratigraphy in this section of core IG-KSF-11 suggests that collected glauconite grains were formed *in situ*. There is no evidence for gravity-induced sediment deposition in this part of the margin. At the Demerara margin, glauconite grains mostly occur as internal fillings of foraminifera. The grains were isolated under the microscope

[1]https://doi.org/10.17600/13010030

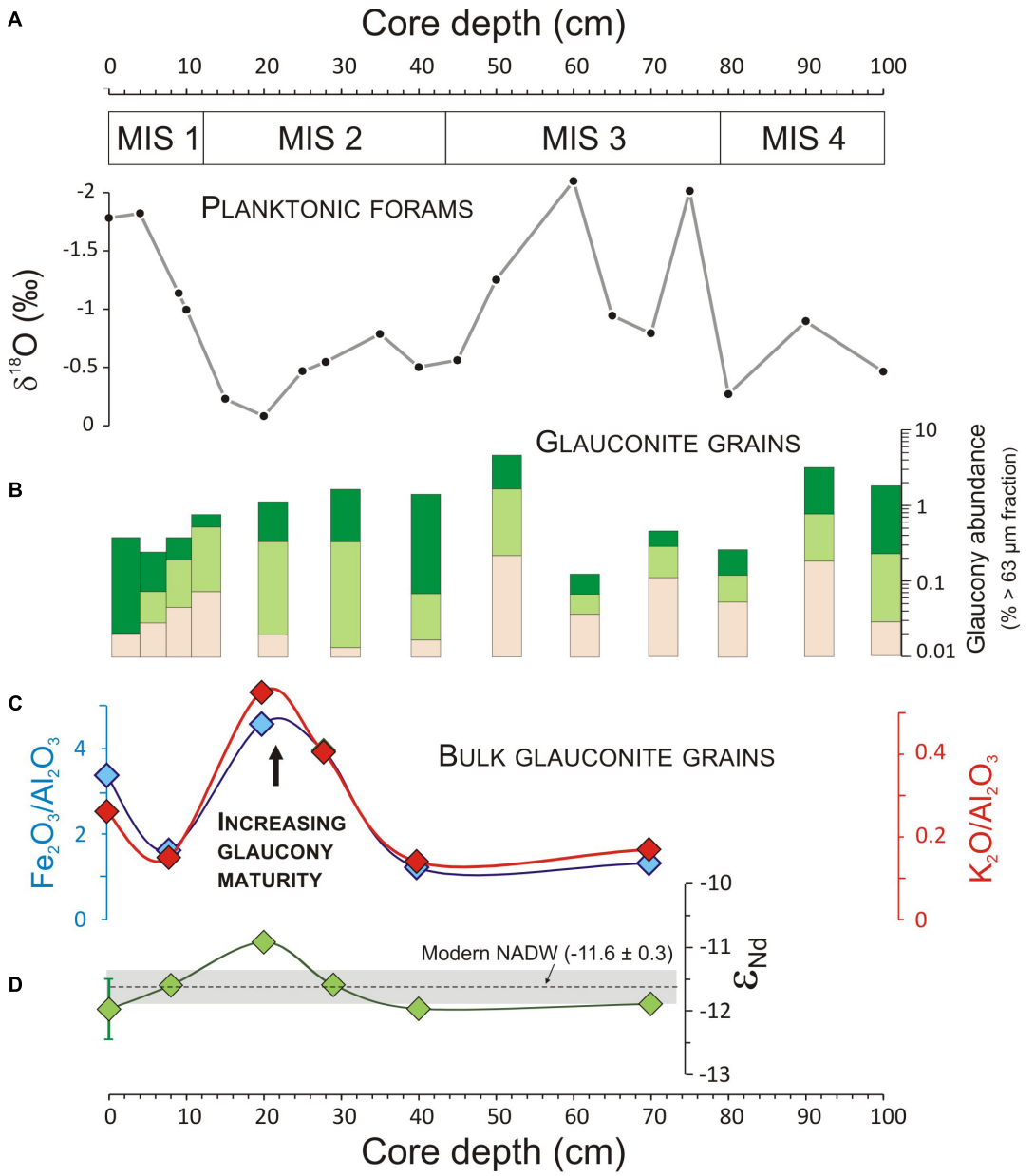

FIGURE 3 | (A) Planktonic foraminifer $\delta^{18}O$ depth profile (Tallobre et al., 2019) and **(B)** relative abundance distribution of glauconitic grains in core IG-KSF-11 (Tallobre et al., 2019). The beige, light green, and dark green boxes correspond to increasing degrees of glauconitic maturity based on visual colour and number of cracks. **(C)** Bulk Fe_2O_3/Al_2O_3 and K_2O/Al_2O_3 ratios of studied glauconite grains (this study), reflecting the degree of glauconitisation. **(D)** Nd isotopic composition (ε_{Nd}) of bulk glauconite grains. The dotted line and associated grey band indicates the present-day ε_{Nd} value of ambient bottom-waters at the same water depth (Huang et al., 2014). Note that the uncertainty on measured ε_{Nd} values (±0.15; 2 SD) is smaller than symbol size, unless reported (sample 0_1 cm).

and were then classified into three main colour categories: (1) beige/grey, (2) light green/green, and (3) dark green (**Figure 4**). Representative samples of each category were selected for SEM observation, using a SEM HITACHI S-4500 (University of Perpignan). Microprobe chemical microanalyses were performed on hemispherical sections obtained after grains were broken. Scanning was performed on both 100 and 2 μm^2 areas in order to obtain representative semi-quantitative analyses of bulk grains and newly formed nano-crystallites.

For geochemical and Nd isotope analyses of glauconite grains, a few grains of ~300–400 µm size were used. Between 30 and 90 mg of powdered sample were digested on hotplate (120°C; 1 day) with distilled 6 M HCl, following a procedure adapted from Yadav and Sharma (1992). This method achieves efficient preferential dissolution of glauconite, yielding almost quantitative recovery of K, while leaving behind more resistant Al- and Si-rich silicate minerals. This implies that major element abundances and ratios (e.g., K_2O/Al_2O_3 and Fe_2O_3/Al_2O_3; see

TABLE 1 | Major (wt %), rare earth elements (μg/g), and Nd isotopic composition of glauconitic grains.

Sample depth	Age	Fe_2O_3	MgO	Al_2O_3	K_2O	CaO	P_2O_5	MnO	Y	La	Ce	Pr	Nd	Sm	Eu	Gd	Tb	Dy	Ho	Er	Yb	Lu	Y/Ho	$^{143}Nd/^{144}Nd$	2 se (10^{-6})	$\varepsilon_{Nd} \pm 2sd$	
0–1 cm	MIS 1	23.48	3.38	6.96	1.82	9.09	0.91	0.04	5.06	11.87	11.87	2.74	10.20	1.96	0.42	1.72	0.18	1.03	0.18	0.48	n.d.	0.08	28.8	0.512021	± 24	−12.0	± 0.5
8–9 cm	MIS 1	18.41	2.62	11.37	1.72	1.91	0.12	0.04	5.04	19.21	33.52	3.87	13.48	2.30	0.41	1.62	0.19	1.05	0.18	0.46	0.42	0.06	27.5	0.512040	± 7	−11.7	± 0.2
20–21 cm	MIS 2	26.95	3.51	5.89	3.24	3.79	0.15	0.04	3.45	8.33	15.72	1.96	7.29	1.38	0.27	1.09	0.13	0.71	0.13	0.30	0.30	0.04	27.5	0.512075	± 9	−11.0	± 0.2
29–30 cm	MIS 2	24.99	3.05	6.32	2.57	2.44	0.15	0.03	2.71	8.39	15.12	1.82	6.59	1.21	0.23	0.83	0.10	0.56	0.10	0.26	0.25	0.03	28.2	0.512041	± 8	−11.7	± 0.2
40–41 cm	MIS 2/3	16.12	2.68	13.23	1.87	1.60	0.13	0.03	5.51	21.80	37.89	4.40	15.08	2.63	0.49	1.89	0.21	1.16	0.20	0.51	0.42	0.06	27.5	0.512021	± 6	−12.0	± 0.2
70–71 cm	MIS 3	17.28	2.67	13.15	2.24	1.50	0.13	0.03	5.30	22.36	22.36	4.45	15.24	2.62	0.45	1.71	0.19	1.06	0.19	0.48	0.40	0.05	28.0	0.512025	± 7	−12.0	± 0.2
WRAS[a]		5.71	1.66	13.8	2.26	0.94	0.84	0.03	29.40	37.80	77.69	8.77	32.69	6.15	1.19	5.19	0.82	4.95	1.02	2.97	3.01	0.46	29				

[a]*World River Average Silt (WRAS; Bayon et al., 2015).*

TABLE 2 | Nd isotopic composition of unclean foraminifers, leached Fe-Mn oxyhydroxide phases, and detrital clays.

Sample depth	Age	$^{143}Nd/^{144}Nd$		2 se (10^{-6})	$\varepsilon_{Nd} \pm 2sd$		
Unclean foraminifers							
0–1 cm	MIS 1	0.512079	±	8	−10.9	±	0.2
8–9 cm	MIS 1	0.512087	±	8	−10.7	±	0.2
20–21 cm	MIS 2	0.512116	±	5	−10.2	±	0.2
29–30 cm	MIS 2	0.512103	±	12	−10.4	±	0.2
40–41 cm	MIS 2/3	0.512095	±	9	−10.6	±	0.2
70–71 cm	MIS 3	0.512083	±	8	−10.8	±	0.2
Leached Fe-Mn oxyhydroxides							
4–5 cm	MIS 1	0.512165	±	9	−9.2	±	0.2
9–10 cm	MIS 1	0.512160	±	6	−9.3	±	0.2
20–21 cm	MIS 2	0.512173	±	4	−9.1	±	0.2
28–29 cm	MIS 2	0.512160	±	8	−9.3	±	0.2
40–41 cm	MIS 2/3	0.512168	±	5	−9.2	±	0.2
50–51 cm	MIS 3	0.512173	±	6	−9.1	±	0.2
60–61 cm	MIS 3	0.512163	±	5	−9.3	±	0
70–71 cm	MIS 3	0.512165	±	8	−9.2	±	0
80–81 cm	MIS 4	0.512197	±	8	−8.6	±	0
Detrital clay-rich fractions (<4 μm)							
4–5 cm	MIS 1	0.512060	±	8	−11.3	±	0.2
9–10 cm	MIS 1	0.512046	±	5	−11.6	±	0.2
20–21 cm	MIS 2	0.512051	±	6	−11.5	±	0.2
28–29 cm	MIS 2	0.512050	±	7	−11.5	±	0.2
40–41 cm	MIS 2/3	0.512055	±	6	−11.4	±	0.2
50–51 cm	MIS 3	0.512065	±	5	−11.2	±	0.2
60–61 cm	MIS 3	0.512073	±	7	−11.0	±	0
70–71 cm	MIS 3	0.512043	±	7	−11.6	±	0
80–81 cm	MIS 4	0.512062	±	6	−11.2	±	0

section "Discussion") reported here for glauconitic grains may slightly differ from values that would otherwise be obtained for bulk glauconite digested using HF-based mineralisation methods. For the analyses of foraminiferal tests, about 10–15 mg of mixed planktonic foraminifera assemblages was prepared using the methodology described in Tachikawa et al. (2014), being dissolved using dropwise addition of ultrapure 1 M acetic acid in order to reduce any potential leaching of associated silicate detritus.

In addition, a total of nine bulk sediment samples from the same core interval were processed for isolating Fe-Mn oxyhydroxide phases and detrital clays. Bulk sediments were first treated using a sequential leaching procedure (Bayon et al., 2002) that successively removes biogenic carbonates (with 5% v/v acetic acid), Fe-Mn oxyhydroxide phases (with a mixed 15% acetic acid—0.5 M hydroxylamine hydrochloride solution) and organic matter (with 15% v/v hydrogen peroxide). For Fe-Mn oxyhydroxide phases, the resulting leachates were filtered through 0.45 μm PTFE Nalgene filters, evaporated to dryness, and finally redissolved using ultrapure HNO_3 prior to subsequent elemental analyses. Clay-rich detrital fractions (<4 μm) were separated from the residual detrital material using low-speed centrifugation (Bayon et al., 2015) and further digested by alkaline fusion (Bayon et al., 2009).

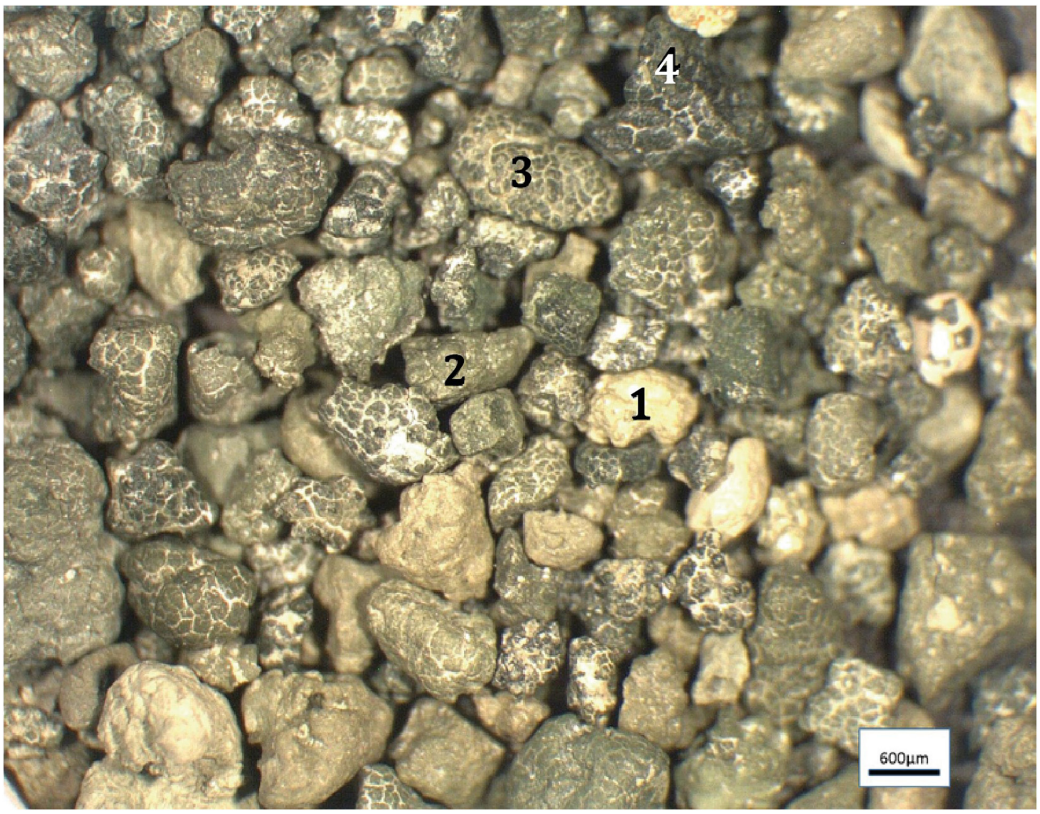

FIGURE 4 | Photograph showing the various degrees of glauconitic maturity inferred from colour and characteristic cracks. (1) Beige grains; (2) light green grains; (3) light green grains with cracks; and (4) dark green grains with cracks.

Major and trace element analyses for 6 M HCl digests of glauconite grains were determined at the Pôle Spectrométrie Océan (PSO, Brest) with a Thermo Scientific Element XR sector field ICP-MS, using the following masses (^{24}Mg, ^{27}Al, ^{31}P, ^{39}K, ^{44}Ca, ^{55}Mn, and ^{57}Fe) acquired in medium mass resolution. Yttrium and REE concentrations were also measured in low resolution mode. Elemental abundances were calculated using the Tm addition method, following the procedures described in Barrat et al. (1996, 2012). The internal precision for all measurements was better than 2%. The precision and accuracy of our data were assessed by analysing a series of silicate rock certified reference materials (CRM) having various chemical compositions (AN-G, AGV-1, BCR-1, DNC-1, DR-N, G-2, and WS-E), digested using conventional HF-HCl-HNO_3 method. The results obtained for these reference materials were in full agreement with reference values from the literature (typically < 8%), with precisions generally better than 10% (RSD; n = 3 for all of the CRMs). Neodymium was isolated using conventional ion chromatography, and isotopic measurements were performed at the PSO-Brest, using a Thermo Scientific Neptune multi-collector ICPMS. Nd isotopic compositions were determined using sample-standard bracketing, by analysing an in-house standard solution (SPEX-Nd) every two samples, yielding a mean value of 0.511687 ± 0.000007 (2 SD, n = 14). Mass bias corrections were made with the exponential law, using ^{146}Nd/^{144}Nd = 0.7219. Analyses of the JNdi-1 standard solution during the course of this study gave ^{143}Nd/^{144}Nd of 0.512114 ± 0.000010 (2 SD, n = 8), in full agreement with the reference value of 0.512115 (Tanaka et al., 2000), and corresponding to an external reproducibility of ∼ ± 0.2 ε (2 SD). Note that epsilon Nd values [$\varepsilon_{Nd} = (^{143}Nd/^{144}Nd_{SAMPLE}/^{143}Nd/^{144}Nd_{CHUR} - 1) \times 10^4$] were calculated using the chondritic (CHUR) ^{143}Nd/^{144}Nd value of 0.512638 (Jacobsen and Wasserburg, 1980).

RESULTS

Microscopic Observations and SEM Microanalyses

As a general rule, the maturity process of glauconitisation is indicated by darker colour and deeper cracks at the grain surface (Giresse and Wiewióra, 2001; Giresse, 2008). Therefore, to a first approximation, both the grain colour and its facies can be used to infer the successive stages of glauconitisation in sedimentary records (**Figure 4**). This descriptive approach was already used by Tallobre et al. (2019), indicating that maximum abundance of mature dark green grains in core IG-KSF-11 generally occurred during MIS 2 (between *ca.* 19–29 kyr BP) and in MIS 4 (∼60–70 kyr BP), in sediment layers also characterised

by high contents of glauconitic grains indicative of enhanced winnowing conditions (**Figure 3B**). Another layer containing relatively high abundance of dark green mature grains is also encountered near the top of the core of Early Holocene age, where the series is extremely condensed (**Figure 3B**). The geochemical results obtained from newly acquired SEM/EDS microanalyses of glauconite grains are listed in **Supplementary Table 1** (Al_2O_3, K_2O, Fe_2O_3, and MgO) and illustrated in **Figures 5**, **6**. These data indicate that at the microscopic scale neoformed microcrystals of dark green grains can yield K_2O and Fe_2O_3 concentrations of up to 8 and 42%, respectively (**Figure 5** and **Supplementary Table 1**). The average Al_2O_3 concentrations in studied glauconitic grains progressively decrease with the degree of maturity of the grains, from 10.1 ± 2.4% (light-coloured grains; n = 17), 6.4 ± 1.6% (green grains; n = 39), and 5.1 ± 2.3% (dark green grains; n = 11). By contrast, both

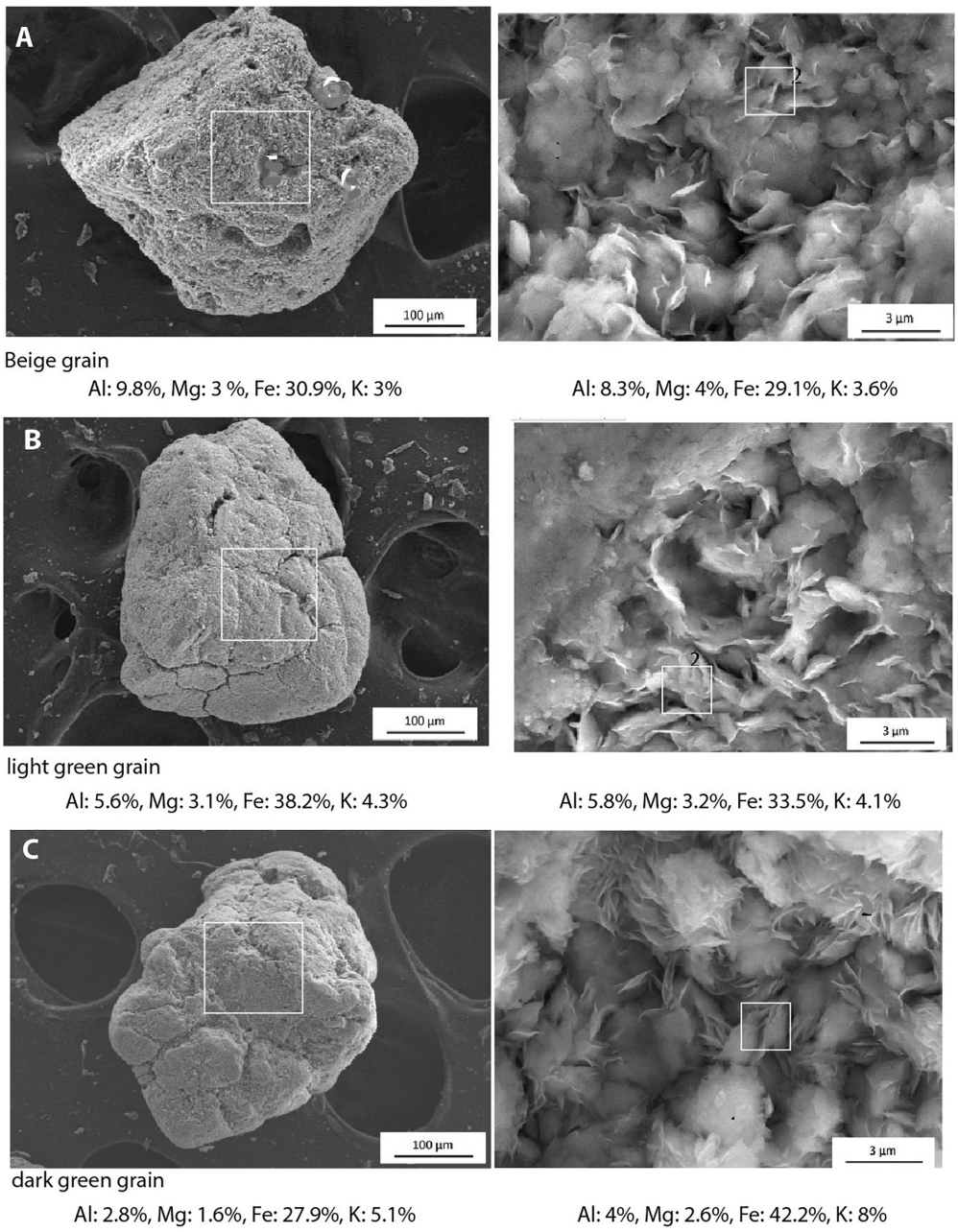

FIGURE 5 | Structural, microstructural, and chemical compositions of the successive glauconitic sequence in core IG-KSF-11. **(A)** Beige grain exhibiting high porosity (left side), showing microstructural evidence of neoformed glauconitic microcrystals (right side). **(B)** Light green grain with minor cracks (left side), exhibiting honeycomb development of newly formed microcrystals (right side). **(C)** Hummocky dark green grain with marked cracks (left side), showing high density of newly formed microcrystals (right side). Note that the white squares indicate microscanned SEM/EDS areas, with corresponding chemical compositions.

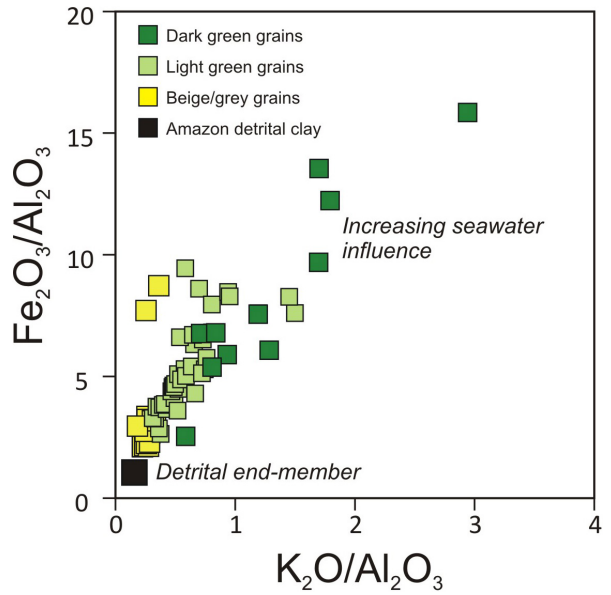

FIGURE 6 | Relationship between Fe_2O_3/Al_2O_3 and K_2O/Al_2O_3 in glauconitic grains of core IG-KSF-11, based on SEM/EDS microanalyses. Values for Amazon detrital clay are from Bayon et al. (2015).

K_2O abundances increase from 2.7 ± 0.7% (light-coloured) to 3.7 ± 0.8% (green) and 5.7 ± 1.1%, similar to Fe_2O_3: 29.1 ± 4.0% (light-coloured) to 32.1 ± 3.7% (green) and 35.9 ± 4.2% (**Supplementary Table 1**). Finally, measured MgO contents remain near constant in beige and light green grains (2.4–4.3%), but decrease in dark green grains (1.1–2.6%; **Supplementary Table 1**) due to progressive replacement of 2:1 (Te-Oc-Te) layers of montmorillonite by glauconite.

Major and Trace Elements and Nd Isotopic Compositions of Glauconitic Grains

The major and trace element concentrations obtained for HCl digests of glauconitic grains are listed in **Table 1**, together with corresponding Nd isotopic compositions. Measured concentrations are reported relative to the initial mass of bulk glauconite grain prior to 6 M HCl digestion. The HCl digests display Fe_2O_3 and Al_2O_3 concentrations ranging from 16.1 to 15.0% and 5.9 to 13.2 wt%, respectively. Potassium (K_2O) concentrations vary from 1.7 to 3.2 wt%, while CaO and P_2O_5 range from 1.5 to 9.1% and 0.1 to 0.9 wt%, respectively. The major element data are also expressed using K_2O/Al_2O_3 and Fe_2O_3/Al_2O_3 ratios (**Figure 3C**). The REE display abundances significantly lower than those for typical detrital sediments, with Nd ranging between ∼6 and 15 μg/g. Measured REE concentrations are also reported as shale-normalised patterns using values for World River Average Silt (WRAS; Bayon et al., 2015), displaying marked light-REE enrichments relative to mid- and heavy-REE (**Figure 7**). The Nd isotopic compositions vary from ε_{Nd} −12.0 (at 0–1 and 40–41 cm depth) to −11.0 (at 20–21 cm) (**Figure 3D**). In comparison, the ε_{Nd} values determined in corresponding uncleaned foraminifers (between −10.9 and −10.2) and leached sedimentary Fe-Mn oxyhydroxide phases (between −9.3 and −8.6) are significantly more radiogenic (**Table 2**). Finally, the Nd isotopic composition of the detrital clay-rich fraction is relatively homogenous along core IG-KSF-11 (between −11.6 and −11.0), with a mean ε_{Nd} signature of −11.4 ± 0.2 (1SD).

DISCUSSION

Glauconitisation at the Demerara Margin

As already shown in Tallobre et al. (2019), the new SEM-EDS data reported in this study indicate that the glauconitic grains formed at site IG-KSF-11 progressively evolve towards darker green shades as they incorporate higher amounts of Fe and K (**Figures 5**, **6**). Successive glauconite neoformation steps are also accompanied by a gradual decrease in Al contents, generally reflecting the gradual disappearance of inherited terrigenous 1:1 minerals, such as kaolinite. By contrast, the corresponding increase in K_2O and Fe_2O_3 is largely independent of the presence of inherited minerals. The source of K in glauconite is directly derived from ambient bottom water, being sequestered between newly formed and/or transformed micaceous sheets. The abundance of K_2O thus directly reflects the process of glauconitogenesis (Odin and Fullagar, 1988; Wiewióra et al., 2001). In the case of core IG-KSF-11, the increase in K_2O contents, and by inference K_2O/Al_2O_3 ratios (**Figure 5**), most likely corresponds to the presence of neoformed sheets of 2:1 clay minerals, such as K-bearing montmorillonite and illite.

In core IG-KSF-11, the abundance of the different types of glauconite grains displays clear correlation with corresponding $\delta^{18}O$ records for both planktonic and benthic foraminifers over the last three isotopic stages (**Figure 3**; Tallobre et al., 2019). The maximum abundance of glauconite grains in the 15–60 and 90–100 cm core intervals of IG-KSF-11 (expressed by the relative weight glauconitic green grains within the sandy fraction; Tallobre et al., 2019) coincides with the glacial periods of MIS 2 and MIS 4, respectively (**Figure 3**). These enriched glauconitic layers were interpreted as reflecting periods characterised by intense winnowing effect, which prevented the burial of the glauconitic grains at that time, favouring their mineralogical evolution at the water–sediment interface. Overall, the occurrence of both higher concentrations of glauconitic grains, higher relative abundances of dark green grains, and higher K_2O/Al_2O_3 and Fe_2O_3/Al_2O_3 ratios (**Figure 3**) collectively point towards a higher dynamics of contouritic currents during MIS 2 and MIS 4, in agreement with what had been proposed by Tallobre et al. (2019).

Core-Top Evidence for a Seawater-Derived Nd Isotopic Signature in Glauconite

A striking feature is the evidence that core-top glauconitic grains at site IG-KSF-11 display a similar Nd isotopic composition

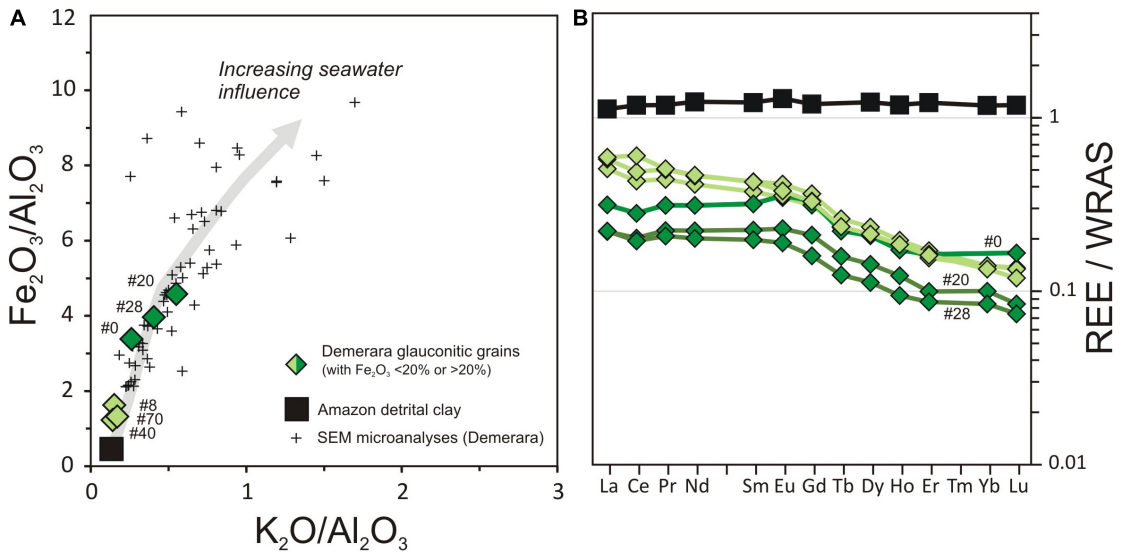

FIGURE 7 | (A) Relationship between Fe_2O_3/Al_2O_3 and K_2O/Al_2O_3 for bulk glauconitic grains from core IG-KSF-11 (diamonds), compared to microscale results obtained by SEM/EDS analyses (crosses). **(B)** Shale-normalised REE patterns of bulk glauconitic grains. WRAS refers to World River Average Silt (Bayon et al., 2015). Note that # refers the sample depth (cm). Values for Amazon detrital clay are from Bayon et al. (2015).

(−12.0 ± 0.5) than that of the corresponding water mass at the Demerara margin (−11.6 ± 0.3; Huang et al., 2014; **Figure 2**). This finding suggests that in highly dynamic depositional environments, characterised by high bottom current velocity, glauconite grains may capture the Nd isotopic composition of ambient bottom water masses. While radiocarbon dating of planktonic foraminifera assemblages suggested possible loss of the surficial sediment layer upon core recovery, the upper 10 cm of core IG-KSF-11 is still assumed to correspond to the Holocene period, hence covering a period of time during which bottom water ε_{Nd} signatures are expected to have remained near present-day values. In marked contrast, both uncleaned foraminifera (−10.9 ± 0.1; 0–1 cm depth) and leached sedimentary Fe-Mn oxyhydroxide (−9.2 ± 0.2; 4–5 cm depth) fractions from the same upper sediment layer depart significantly from the expected NADW-like Holocene seawater signature. Neodymium isotopic measurements on uncleaned foraminifera are usually assumed to reflect the signature of associated Fe-Mn oxyhydroxide coatings that precipitate onto and within the foraminifera tests at the seawater–sediment interface (e.g., Elmore et al., 2011; Tachikawa et al., 2014), hence acquiring the ε_{Nd} composition of ambient bottom waters. The fact that core-top foraminifera at site IG-KSF-11 do not match similar Nd isotopic composition than the overlying water mass suggests that they were initially derived from another depositional environment, before being transported to site IG-KSF-11 by erosion and subsequent bottom current transport. Considering the ε_{Nd} distribution along the water column at the Demerara Rise (Huang et al., 2014; **Figure 2**), we infer that the foraminifera assemblages encountered in the contourite moat at site IG-KSF-11 may be possibly derived from shallower depositional environments, at water depths between 600 m and 800 m bathed by AAIW.

While Fe-Mn oxyhydroxide phases leached from bulk marine sediments are commonly used as paleoceanographic archives (e.g., Rutberg et al., 2000; Piotrowski et al., 2005; Gutjahr et al., 2008), the Fe-oxide fractions extracted from continental margin sediment records can also include pre-formed continental oxides associated with terrigenous material (e.g., Bayon et al., 2004; Kraft et al., 2013; Jang et al., 2020), hence complicating their use for reconstructing past ocean circulation. In this study, the evidence that leached Fe-oxyhydroxide phases significantly depart from NADW-like ε_{Nd} values clearly point towards the presence of such pre-formed continental oxides. In fact, recent investigations have shown that river-borne Fe oxides are almost systematically characterised by more radiogenic Nd isotopic compositions relative to the associated detrital material (Hindshaw et al., 2018; Bayon et al., 2020; Jang et al., 2020). This Nd isotope decoupling between paired Fe oxide and detrital silicate fractions has been attributed to the preferential erosion and/or weathering of sedimentary rocks on continents (e.g., Bayon et al., 2020). For instance, recent sediments deposited near the mouth of the Amazon River display ε_{Nd} values of −8 and −10.7 for leached Fe oxides and detrital fractions, respectively (Bayon et al., 2020). At the Demerara Rise, the main potential sources of sediment include suspended particulate material from the large South American tropical rivers (Amazon, Orinoco, and Maroni) that are subsequently transported by ocean currents. These different sources display pronounced ε_{Nd} compositional variability, which can be used to trace the origin of the lithogenic material deposited on adjacent ocean margins (Rousseau et al., 2019). For instance, over the hydrological year, the Amazon River exhibits particulate ε_{Nd} values ranging from −9.8 to −11.4 (mean −10.6 ± 0.6) while the suspended loads of the Orinoco and the Maroni yield −14.1 ± 0.3 and −23.7 ± 1.2, respectively. By analogy and in agreement with previous studies (Häggi et al., 2017;

Zhang et al., 2017; Crivellari et al., 2018), we infer that measured Nd isotopic compositions for both detrital (-11.4 ± 0.2) and Fe-oxide (-9.1 ± 0.2) fractions in core IG-KSF-11 possibly reflect the dominant presence of Amazon sediments at the studied site.

Taken together, the above findings hence suggest that in highly dynamic environments at continental margins, such as the Demerara Rise, glauconitic grains may be best suited than foraminifera and leached sedimentary Fe-oxides for reconstructing the Nd isotopic composition of ambient bottom water masses.

Mode of Acquisition of Ambient Seawater ε_{Nd} Signatures by Glauconitic Grains

In contrast with Nd isotopes, which suggest a seawater origin for the core-top glauconitic grains at site IG-KSF-11, the distribution of REE in studied grains is far more equivocal, suggesting a complex mode of acquisition of ambient bottom water ε_{Nd} signatures. For instance, Y/Ho, i.e., a proxy for the relative contribution of seawater versus terrestrial signatures in marine sediments (Nozaki et al., 1997) displays values (27.9 ± 0.5; **Table 1**) indistinguishable from detrital river sediments worldwide (WRAS; 28.7 ± 1.3; Bayon et al., 2015), far from the range of seawater values (Y/Ho > ∼40–70; Bau, 1996). To some extent, this finding could indicate that the initial acquisition of REE by glauconitic grains is set by the dissolution of clay minerals, being modified subsequently by sustained isotopic exchange with seawater. Albeit different, such a process would echo with previous investigations that already suggested that fine-grained particles settling in the ocean could interact with seawater through intense dissolved-particle exchange, resulting in no significant Nd enrichment but overall leading to the acquisition of seawater Nd isotopic signatures (e.g., Jeandel et al., 1995; Tachikawa et al., 1997). In marine environments, glauconitisation involves successive dissolutions of dominant 1:1 and subsequent 2:1 clay minerals (smectite), followed by neoformation of other 2:1 micaceous sheets of glauconite. As mentioned above, the process of glauconitisation is accompanied by the loss of several cations (Al and even Si) and the enrichment of other major elements such as Fe and K. Dissolution can also occur when the starting clay phase is mainly composed of 1:1 clay minerals, such as kaolinite. For example, in the case of Fe-bearing montmorillonite green grains from the Ivory Coast-Ghana marginal ridge (ODP Site 359), kaolinite was shown to dissolve slowly with remnants of d (001) and d (060) peaks of kaolinite being still present in the pristine light coloured grains (Wiewióra et al., 2001). At the Demerara Rise, this process can also be illustrated using Fe_2O_3/Al_2O_3 versus K_2O/Al_2O_3 ratios determined in bulk glauconite grains (**Figure 7**), where the observed positive relationship (which perfectly matches with the correlation defined by SEM/EDS data; **Figure 6**) indicates increasing glauconitisation and seawater influence as both Fe_2O_3/Al_2O_3 and K_2O/Al_2O_3 ratios increase. In core IG-KSF-11, the highest Fe and K concentrations are encountered in grains formed during MIS 2 (at 20 and 28 cm depth), in full agreement with the preferential abundance of dark green grains in the corresponding sediment interval, indicative of greater degree of glauconitisation and a longer residence time due to strengthened bottom current activity.

Interestingly, the shale-normalised REE patterns of the green glauconite grains extracted from our Demerara contourite sediments indicate that increasing degrees of glauconitisation is accompanied by a net loss in REE (**Figure 7**). This finding echoes with previous works conducted on glauconitic grains of both Recent (Stille and Clauer, 1994) and Cenozoic (Tóth et al., 2010) ages, which reported similar observations that the REE contents of glauconite grains gradually decrease during glauconitisation. These latter authors proposed that the progressive REE loss during glauconitisation directly resulted from the crystallographic transformation of the phyllosilicate layers, leading to the combined depletion of both Ca and REE (Tóth et al., 2010). Additionally, one striking feature of the studied glauconitic grains from core IG-KSF-11 is that they display apparent LREE enrichment relative to MREE and HREE, resulting in shale-normalised patterns that depart significantly from both the typical seawater and detrital distribution patterns (**Figure 7**). As previously proposed, this particular REE signature could possibly relate to the presence of discrete authigenic REE-rich phosphate phases, such as cryptocrystalline apatite, which are typically found in close association with green glauconite grains in the sedimentary record (Stille and Clauer, 1994; Wigley and Compton, 2007; Tóth et al., 2010; Huggett et al., 2017). Present as inclusions within glauconitic grains, these authigenic REE-rich phosphate phases are thought to play an important role in controlling the REE budget of glauconitic grains (Stille and Clauer, 1994; Tóth et al., 2010). At the Demerara margin, studied grains display no direct correlation between both P_2O_5 and REE contents (**Table 2**), possibly suggesting that the REE composition of accessory phosphate phases may vary substantially amongst glauconitic grains. Nevertheless, based on the above consideration, we propose that the presence of such discrete authigenic phosphate minerals most likely explain why glauconitic grains at the Demerara margin can faithfully record the Nd isotopic composition of ambient bottom waters. In any case, our results suggest that increasing glauconite maturity results in progressive loss of the ε_{Nd} signature of inherited clay minerals, most likely accompanied by a gradual shift towards seawater Nd isotope composition. To some extent, this finding would also be in agreement with the evidence that other authigenic phosphate mineral phases (hydroxyfluorapatite), which control the REE budget of fish teeth following their deposition at seafloor, also act as reliable recorders of the Nd isotopic composition of bottom waters (e.g., Martin and Haley, 2000; Martin and Scher, 2004).

Preliminary Paleoceanographic Implications

As mentioned above, the occurrence of both higher concentrations of glauconitic grains and increasing relative abundances of more evolved dark green grains during MIS 2 has been interpreted as reflecting a strengthening of bottom water circulation along the Demerara margin during glacial times

(Tallobre et al., 2019). Since the studied site is located in the core interval of the modern NADW, at a water depth of ∼2400 m, this finding was taken as evidence for an intensification of the glacial AMOC. This hypothesis was in agreement with recent ε_{Nd}-based paleoceanographic reconstructions, which suggested sustained production of glacial NADW during the last glacial period (Howe et al., 2016; Pöppelmeier et al., 2020). Our newly acquired data also provide additional support for a vigorous flow of the glacial analogue of NADW at the Demerara margin. First, our major element data for bulk glauconite grains further indicate that glauconitisation was enhanced at that time as inferred from significant enrichments in Fe and K in neoformed glauconitic minerals, hence also pointing towards intensifying winnowing during glacial periods (**Figure 3C**). Second, our Nd isotope data for the glauconitic grains formed during MIS 2 (**Figure 3D**) indicate no major change in the ε_{Nd} signature of ambient bottom water masses during glacials (between −11.0 and −11.7) relative to their present-day composition (−11.6 ± 0.3; Huang et al., 2014). The evidence that the glacial NADW flowing along the Demerara margin was slightly more radiogenic compared to the modern NADW ε_{Nd} signature could be explained by the fact that northern-sourced waters may have acquired a distinctive Nd isotopic composition at that time (−10.4 ± 1.0), reflecting the impact of ice sheets on nearby continents on the release of dissolved Nd to the North Atlantic (Zhao et al., 2019). This finding is in agreement with the results obtained by Huang et al. (2014) on uncleaned foraminifera extracted from a nearby shallower sediment core (∼950 m), which also indicated similar ε_{Nd} composition for the overlying AAIW during the Holocene and the LGM. Taken together, these two ε_{Nd} records hence collectively suggest that the structure of the water column at the Demerara margin during glacial times was probably similar to its modern oceanographic configuration.

CONCLUSION AND PERSPECTIVES

Our geochemical investigation of glauconitic grains recovered from a contourite sediment sequence at the Demerara margin suggests that authigenic glauconite can faithfully record the Nd isotopic composition of ambient bottom water masses. The acquisition of ε_{Nd} seawater signatures in glauconitic grains appears to be controlled by the presence of LREE-enriched phases, possibly corresponding to dispersed authigenic phosphate phases intertwined within the neoformed clay mineral sheets. The absence of a strong detrital control on measured Nd isotopic compositions in glauconite grains is further inferred from the evidence for a progressive loss of REE with increasing degrees of glauconitisation; a process that also results in gradual enrichments in Fe and K. Overall, our new results suggest that the application of Nd isotopes to glauconite grains could serve as useful proxies for paleoceanographic reconstructions at continental margins, wherever intense winnowing and/or erosional processes may prevent the use of other more conventional archives of past seawater ε_{Nd} compositions, such as uncleaned foraminifera or leached Fe-Mn oxyhydroxide fractions. In particular, the combined use of Nd isotopes (as tracers of water mass) and various elemental ratios, such as Fe_2O_3/Al_2O_3 and K_2O/Al_2O_3 (as tracers for the degree of glauconitisation), could provide complementary information of both the source and strength of past bottom water circulation. An important requisite prior to establishing Nd isotopes in glauconite grains as robust paleoceanographic archives will be to further demonstrate the preliminary findings reported in this study, by investigating additional sites from the Demerara Rise or from any other contourite systems where bottom water masses and local detrital sediment may display contrasted Nd isotopic compositions.

DATA AVAILABILITY STATEMENT

The original contributions presented in the study are included in the article/**Supplementary Material**. Further inquiries can be directed to the corresponding author/s.

AUTHOR CONTRIBUTIONS

PG and GB contributed to the conception and design of the study and wrote the manuscript with contributions from all authors. CT contributed to the first visual analysis and counting of glauconitic grains in core IKSF11. PG and CT prepared the glauconitic grains and conducted SEM observations and analyses. GB performed all REE and Nd isotopic compositions. LL was the head scientist of the IGUANES cruise allowing the acquisition of IKSF11 core and contributed to the regional understanding of the study area. All authors contributed to the article and approved the submitted version.

FUNDING

The geochemical analyses were performed through internal funding at IFREMER.

ACKNOWLEDGMENTS

We thank the crews of R/V *L'Atalante* and all participants of the IGUANES cruise (2013; Chief scientist: Lies Loncke, https://doi.org/10.17600/13010030) for their assistance at sea. We are most grateful to Alexis De Prunelé for assistance during MC-ICPMS measurements. We also greatly thank two reviewers for providing insightful and constructive comments, together with CM for editorial handling.

SUPPLEMENTARY MATERIAL

The Supplementary Material for this article can be found online at: https://www.frontiersin.org/articles/10.3389/feart.2021.652501/full#supplementary-material

REFERENCES

Banerjee, S., Bansal, U., and Vilas Thorat, A. (2016). A review on palaeogeographic implications and temporal variation in glaucony composition. *J. Palaeogeogr.* 5, 43–71. doi: 10.1016/j.jop.2015.12.001

Barrat, J. A., Keller, F., Amossé, J., Taylor, R. N., Nesbitt, R. W., and Hirata, T. (1996). Determination of rare earth elements in sixteen silicate reference samples by ICP-MS after Tm addition and ion exchange separation. *Geostand. Newslett.* 20, 133–139. doi: 10.1111/j.1751-908x.1996.tb00177.x

Barrat, J. A., Zanda, B., Moynier, F., Bollinger, C., Liorzou, C., and Bayon, G. (2012). Geochemistry of CI chondrites: major and trace elements, and Cu and Zn isotopes. *Geochim. Cosmochim. Acta* 83, 79–92. doi: 10.1016/j.gca.2011.12.011

Bau, M. (1996). Controls on the fractionation of isovalent trace elements in magmatic and aqueous systems: evidence from Y/Ho, Zr/Hf, and lanthanide tetrad effect. *Contrib. Min. Petrol.* 123, 323–333. doi: 10.1007/s004100050159

Bayon, G., Barrat, J. A., Etoubleau, J., Benoit, M., Bollinger, C., and Revillon, S. (2009). Determination of Rare Earth Elements, Sc, Y, Zr, Ba, Hf and Th in Geological Samples by ICP-MS after Tm addition and alkaline fusion. *Geostand. Geoanal. Res.* 33, 51–62. doi: 10.1111/j.1751-908x.2008.00880.x

Bayon, G., German, C. R., Boella, R. M., Milton, J. A., Taylor, R. N., and Nesbitt, R. W. (2002). An improved method for extracting marine sediment fractions and its application to Sr and Nd isotopic analysis. *Chem. Geol.* 187, 179–199. doi: 10.1016/s0009-2541(01)00416-8

Bayon, G., German, C. R., Burton, K. W., Nesbitt, R. W., and Rogers, N. (2004). Sedimentary Fe–Mn oxyhydroxides as paleoceanographic archives and the role of aeolian flux in regulating oceanic dissolved REE. *Earth Planet. Sci. Lett.* 224, 477–492. doi: 10.1016/j.epsl.2004.05.033

Bayon, G., Lambert, T., Vigier, N., De Deckker, P., Freslon, N., Jang, K., et al. (2020). Rare earth element and neodymium isotope tracing of sedimentary rock weathering. *Chem. Geol.* 553:119794. doi: 10.1016/j.chemgeo.2020.119794

Bayon, G., Toucanne, S., Skonieczny, C., André, L., Bermell, S., Cheron, S., et al. (2015). Rare earth elements and neodymium isotopes in world river sediments revisited. *Geochim. Cosmochim. Acta* 170, 17–38. doi: 10.1016/j.gca.2015.08.001

Böhm, E., Lippold, J., Gutjahr, M., Frank, M., Blaser, P., Antz, B., et al. (2015). Strong and deep Atlantic meridional overturning circulation during the last glacial cycle. *Nature* 517, 73–76. doi: 10.1038/nature14059

Crivellari, S., Chiessi, C. M., Kuhnert, H., Häggi, C., da Costa Portilho-Ramos, R., Zeng, J. Y., et al. (2018). Increased Amazon freshwater discharge during late Heinrich Stadial 1. *Quat. Sci. Rev.* 181, 144–155. doi: 10.1016/j.quascirev.2017.12.005

Elmore, A. C., Piotrowski, A. M., Wright, J. D., and Scrivner, A. E. (2011). Testing the extraction of past seawater Nd isotopic composition from North Atlantic deep sea sediments and foraminifera. *Geochem. Geophys. Geosyst.* 12:Q09008. doi: 10.1029/2011GC003741

Fanget, A.-S., Loncke, L., Pattier, F., Marsset, T., Roest, W. R., Tallobre, C., et al. (2020). A synthesis of the sedimentary evolution of the Demerara Plateau (Central Atlantic Ocean) from the late Albian to the Holocene. *Mar. Petrol. Geol.* 114:104195. doi: 10.1016/j.marpetgeo.2019.104195

Faugères, J. C., and Mulder, T. (2011). "Contour currents and contourite drifts," in *Deep Sea Sediments, Developments in Sedimentology*, Vol. 63, eds H. Huüneke and T. Mulder (Amsterdam: Elsevier), 149–205. doi: 10.1016/b978-0-444-53000-4.00003-2

Frank, M. (2002). Radiogenic isotopes: tracers of past ocean circulation and erosional input. *Rev. Geophys.* 40, 1–38.

Giresse, P. (1975). Essai de chronomètrie de la glauconitisation dans le Golfe de Guinée; exemple de vitesse diagénétique au Quaternaire supérieur. *C.R. Somm. Seances Soc. Géol. Fr.* 5, 163–164.

Giresse, P. (2008). "Some aspects of diagenesis in contourites," in *Contourites, Developments in Sedimentology*, Vol. 12, eds M. Rebesco and A. Camerlenghi (Amsterdam: Elsevier), 203–221. doi: 10.1016/s0070-4571(08)10012-7

Giresse, P., Gadel, F., Serve, L., and Barusseau, J.-P. (1998). Indicators of climate – and sediment- source variations at Site 959 : implication for the reconstruction of paleoenvironments in the Gulf of Guinea through Pleistocene times. *Proc. Ocean Drill. Prog. Sci. Results* 159, 585–603.

Giresse, P., and Wiewióra, A. (2001). Stratigraphic condensed deposition and diagenetic evolution of green clay minerals in deep water sediments on the Ivory Coast-Ghana Ridge. *Mar. Geol.* 179, 51–70. doi: 10.1016/s0025-3227(01)00193-1

Goldstein, S. L., and Hemming, S. R. (2003). "Long-lived isotopic tracers in oceanography, paleoceanography, and ice-sheet dynamics," in *Treatise on Geochemistry*, Vol. 6, eds H. Elderfield, H. D. Holland, and K. T. Turekian (Oxford: Elsevier-Pergamon), 453–489. doi: 10.1016/b0-08-043751-6/06179-x

Gutjahr, M., Frank, M., Stirling, C. H., Keigwin, L. D., and Halliday, A. N. (2008). Tracing the Nd isotope evolution of North Atlantic deep and intermediate waters in the Western North Atlantic since the Last Glacial Maximum from Blake Ridge sediments. *Earth Planet. Sci. Lett.* 266, 61–77. doi: 10.1016/j.epsl.2007.10.037

Häggi, C., Chiessi, C. M., Merkel, U., Mulitza, S., Prange, M., Schulz, M., et al. (2017). Response of the Amazon rainforest to late Pleistocene climate variability. *Earth Planet. Sci. Lett.* 479, 50–59. doi: 10.1016/j.epsl.2017.09.013

Hindshaw, R. S., Aciego, S. M., Piotrowski, A. M., and Tipper, E. T. (2018). Decoupling of dissolved and bedrock neodymium isotopes during sedimentary cycling. *Geochem. Perspect. Lett.* 8, 43–46. doi: 10.7185/geochemlet.1828

Howe, J. N., Piotrowski, A. M., Noble, T. L., Mulitza, S., Chiessi, C. M., and Bayon, G. (2016). North Atlantic deep water production during the Last Glacial Maximum. *Nat. Commun.* 7, 1–8. doi: 10.1038/ncomms11765

Huang, K. F., Oppo, D. W., and Curry, W. B. (2014). Decreased influence of Antarctic intermediate water in the tropical Atlantic during North Atlantic cold events. *Earth Planet. Sci. Lett.* 389, 200–208. doi: 10.1016/j.epsl.2013.12.037

Huggett, J., Adetunji, J., Longstaffe, F., and Wray, D. (2017). Mineralogical and geochemical characterisation of warm-water, shallow-marine glaucony from the Tertiary of the London Basin. *Clay Min.* 52, 25–50. doi: 10.1180/claymin.2017.052.1.02

Jacobsen, S. B., and Wasserburg, G. J. (1980). Sm-Nd isotopic evolution of chondrites. *Earth Planet Sci. Lett.* 50, 139–155. doi: 10.1016/0012-821X(80)90125-9

Jang, K., Bayon, G., Han, Y., Joo, Y. J., Kim, J. H., Ryu, J. S., et al. (2020). Neodymium isotope constraints on chemical weathering and past glacial activity in Svalbard. *Earth Planet. Sci. Lett.* 542:116319. doi: 10.1016/j.epsl.2020.116319

Jeandel, C., Bishop, J. K., and Zindler, A. (1995). Exchange of neodymium and its isotopes between seawater and small and large particles in the Sargasso Sea. *Geochim. Cosmochim. Acta* 59, 535–547. doi: 10.1016/0016-7037(94)00367-u

Kraft, S., Frank, M., Hathorne, E. C., and Weldeab, S. (2013). Assessment of seawater Nd isotope signatures extracted from foraminiferal shells and authigenic phases of Gulf of Guinea sediments. *Geochim. Cosmochim. Acta* 121, 414–435. doi: 10.1016/j.gca.2013.07.029

Lippold, J., Gutjahr, M., Blaser, P., Christner, E., de Carvalho Ferreira, M. L., Mulitza, S., et al. (2016). Deep water provenance and dynamics of the (de) glacial Atlantic meridional overturning circulation. *Earth Planet. Sci. Lett.* 445, 68–78. doi: 10.1016/j.epsl.2016.04.013

Loncke, L., Maillard, A., Basile, C., Roest, W. R., Bayon, G., Gaullier, V., et al. (2016). Structure of the Demerara passive-transform margin and associated sedimentary processes. Initial results from the IGUANES cruise. *Geol. Soc. Lond. Spec. Pub.* 431, 179–197. doi: 10.1144/sp431.7

Martin, E. E., and Haley, B. A. (2000). Fossil fish teeth as proxies for seawater Sr and Nd isotopes. *Geochim. Cosmochim. Acta* 64, 835–847. doi: 10.1016/s0016-7037(99)00376-2

Martin, E. E., and Scher, H. D. (2004). Preservation of seawater Sr and Nd isotopes in fossil fish teeth: bad news and good news. *Earth Planet. Sci. Lett.* 220, 25–39. doi: 10.1016/s0012-821x(04)00030-5

Nozaki, Y., Zhang, J., and Amakawa, H. (1997). The fractionation between Y and Ho in the marine environment. *Earth Planet. Sci. Lett.* 148, 329–340. doi: 10.1016/s0012-821x(97)00034-4

Odin, G. S., and Fullagar, P. D. (1988). "Geological significance of the glaucony" in *Green Marine Clays. Oolitic Ironstone Facies, Verdine Facies, Glaucony Facies and Celadonite-Bearing Facies. A Comparative Studyeds*, Vol. 45, ed G.S. Odin (Amsterdam: Elsevier), 295–332. doi: 10.1016/s0070-4571(08)70069-4

Odin, G. S., and Matter, A. (1981). De glauconiarum origine. *Sedimentology* 28, 611–641. doi: 10.1111/j.1365-3091.1981.tb01925.x

Pahnke, K., Goldstein, S. L., and Hemming, S. R. (2008). Abrupt changes in antarctic intermediate water circulation over the past 25,000 years. *Nat. Geosci.* 1, 870–874. doi: 10.1038/ngeo360

Piotrowski, A. M., Goldstein, S. L., Hemming, S. R., and Fairbanks, R. G. (2004). Intensification and variability of ocean thermohaline circulation through the last deglaciation. *Earth Planet. Sci. Lett.* 225, 205–220. doi: 10.1016/j.epsl.2004.06.002

Piotrowski, A. M., Goldstein, S. L., Hemming, S. R., and Fairbanks, R. G. (2005). Temporal relationships of carbon cycling and ocean circulation at glacial boundaries. *Science* 307, 1933–1938. doi: 10.1126/science.1104883

Pöppelmeier, F., Blaser, P., Gutjahr, M., Jaccard, S. L., Frank, M., Max, L., et al. (2020). Northern-sourced water dominated the Atlantic Ocean during the Last Glacial Maximum. *Geology* 48, 826–829. doi: 10.1130/g47628.1

Robinson, S., Ivanovic, R., van de Flierdt, T., Blanchet, C. L., Tachikawa, K., Martin, E. E., et al. (2021). Global continental and marine detrital ε_{Nd}: an updated compilation for use in understanding marine Nd cycling. *Chem. Geol.* 567:120119. doi: 10.1016/j.chemgeo.2021.120119

Rousseau, T. C., Roddaz, M., Moquet, J. S., Delgado, H. H., Calves, G., and Bayon, G. (2019). Controls on the geochemistry of suspended sediments from large tropical South American rivers (Amazon, Orinoco and Maroni). *Chem. Geol.* 522, 38–54.

Rutberg, R. L., Hemming, S. R., and Goldstein, S. L. (2000). Reduced North Atlantic deep water flux to the glacial Southern Ocean inferred from neodymium isotope ratios. *Nature* 405, 935–938. doi: 10.1038/35016049

Stille, P., and Clauer, N. (1994). The process of glauconitization: chemical and isotopic evidence. *Contrib. Min. Petrol.* 117, 253–262. doi: 10.1007/bf00310867

Stow, D. A. V., and Faugères, J. C. (2008). "Contourite facies and the facies model," in *Contourites, Developments in Sedimentology*, Vol. 60, eds M. Rebesco and A. Camerlenghi (Amsterdam: Elsevier), 223–256. doi: 10.1016/s0070-4571(08)10013-9

Tachikawa, K., Arsouze, T., Bayon, G., Bory, A., Colin, C., Dutay, J. C., et al. (2017). The large-scale evolution of neodymium isotopic composition in the global modern and Holocene ocean revealed from seawater and archive data. *Chem. Geol.* 457, 131–148. doi: 10.1016/j.chemgeo.2017.03.018

Tachikawa, K., Handel, C., and Dupré, B. (1997). Distribution of rare earth elements and neodymium isotopes in settling particulate material of the tropical Atlantic Ocean (EUMELI site). *Deep Sea Res.* I 44, 1769–1792. doi: 10.1016/s0967-0637(97)00057-5

Tachikawa, K., Piotrowski, A. M., and Bayon, G. (2014). Neodymium associated with foraminiferal carbonate as a recorder of seawater isotopic signatures. *Quat. Sci. Rev.* 88, 1–13. doi: 10.1016/j.quascirev.2013.12.027

Tallobre, C., Giresse, P., Bassetti, M. A., Loncke, L., Bayon, G., Buscail, R., et al. (2019). Formation and evolution of glauconite in the Demerara Contourite depositional system related to NADW circulation changes during late Quaternary (French Guiana). *J. South Am. Earth Sci.* 92, 167–183. doi: 10.1016/j.jsames.2019.03.011

Tallobre, C., Loncke, L., Bassetti, M. A., Giresse, P., Bayon, G., Buscail, R., et al. (2016). Description of a contourite depositional system on the Demerara Plateau: results from geophysical data and sediment cores. *Mar. Geol.* 378, 56–73. doi: 10.1016/j.margeo.2016.01.003

Tanaka, T., Togashi, S., Kamioka, H., Amakawa, H., Kagami, H., Hamamoto, T., et al. (2000). JNdi-1: a neodymium isotopic reference in consistency with LaJolla neodymium. *Chem. Geol.* 168, 279–281. doi: 10.1016/s0009-2541(00)00198-4

Tenzer, R., and Gladkikh, V. (2014). Assessment of density variations of marine sediments with ocean and sediment depths. *Sci. World J.* 2014:9. doi: 10.1155/2014/823296

Tóth, E., Weiszburg, T. G., Jeffries, T., Williams, C. T., Bartha, A., Bertalan, É, et al. (2010). Submicroscopic accessory minerals overprinting clay mineral REE patterns (celadonite–glauconite group examples). *Chem. Geol* 269, 312–328. doi: 10.1016/j.chemgeo.2009.10.006

von Blanckenburg, F. (1999). Tracing past ocean circulation? *Science* 286, 1862–1863.

Wiewióra, A., Giresse, P., Petit, S., and Wilamowski, A. (2001). A deep-water glauconitization process on the Ivory Coast—Ghana marginal ridge (ODP site 959): determination of Fe 3+-rich montmorillonite in green grains. *Clays Clay Min.* 49, 540–558. doi: 10.1346/ccmn.2001.0490606

Wigley, R., and Compton, J. S. (2007). Oligocene to Holocene glauconite–phosphorite grains from the Head of the Cape Canyon on the western margin of South Africa. *Deep Sea Res. II* 54, 1375–1395. doi: 10.1016/j.dsr2.2007.04.004

Yadav, V. P., and Sharma, T. (1992). Leaching of glauconitic sand stone in acid lixiviants. *Miner. Eng.* 5, 715–720. doi: 10.1016/0892-6875(92)90066-i

Zhang, Y., Chiessi, C. M., Mulitza, S., Sawakuchi, A. O., Häggi, C., Zabel, M., et al. (2017). Different precipitation patterns across tropical South America during Heinrich and Dansgaard-Oeschger stadials. *Quat. Sci. Rev.* 177, 1–9. doi: 10.1016/j.quascirev.2017.10.012

Zhao, N., Oppo, D. W., Huang, K. F., Howe, J. N., Blusztajn, J., and Keigwin, L. D. (2019). Glacial–interglacial Nd isotope variability of North Atlantic Deep Water modulated by North American ice sheet. *Nat. Commun.* 10, 1–10. doi: 10.1038/s41467-019-13707-z

Conflict of Interest: The authors declare that the research was conducted in the absence of any commercial or financial relationships that could be construed as a potential conflict of interest.